RSC Advances

COMMUNICATION

View Article Online
View Journal | View Issue

Cite this: *RSC Adv.*, 2016, **6**, 26719

Received 12th February 2016
Accepted 2nd March 2016

DOI: 10.1039/c6ra03905g

www.rsc.org/advances

Nanoscale graphene coating on commercially pure titanium for accelerated bone regeneration†

Ho Sang Jung,[a] Yeong-jin Choi,[b] Jiwon Jeong,[a] Yongmoon Lee,[c] Byungwoo Hwang,[a] Jinah Jang,[b] Jin-Hyung Shim,[d] Yun Seop Kim,[a] Hyun Sik Choi,[a] Sang Ho Oh,[a] Chong Soo Lee,[c] Dong-Woo Cho[e] and Sei Kwang Hahn*[a]

Titanium (Ti) is one of the representative biocompatible metallic materials which has been widely exploited for various implants and bone replacements. Here, commercially pure Ti (CP Ti) was surface-modified with reduced graphene oxide (RGO) for accelerated bone regeneration and osseointegration. Nanoscale RGO coating on CP Ti was clearly confirmed by SEM, AFM, EDS, XPS, HR-TEM and EELS. In addition, pre-osteoblast cells cultured on RGO-CP Ti showed higher cell viability and cell attachment than those on CP Ti. After confirmation of the drug loading capability of RGO-CP Ti, osteogenic dexamethasone loaded RGO-CP Ti (Dex/RGO-CP Ti) was implanted on calvarial bone defects in rats. Synchrotron X-ray imaging successfully visualized more effective bone regeneration on Dex/RGO-CP Ti than CP Ti and RGO-CP Ti after 8 weeks.

Titanium (Ti) has been widely used for the applications to hard tissue engineering due to its excellent biocompatibility, mechanical properties, and resistance to corrosion.[1,2] After implantation, rapid and effective osseointegration at the interface of the Ti implant and bone tissue is one of the most important issues for successful clinical applications.[3] The degree of osseointegration and prognosis is highly dependent on the surface properties of implant materials.[4] In general, roughening of implant surface by machining or acid treatment provided increased surface area for the effective cellular attachment.[5] In addition, bioactive hydroxyapatite coated[6] or biopolymer functionalized Ti surfaces[7] were extensively investigated for bone implant applications. The bioactive surfaces enhanced cell viability, anti-bacterial activity, osseointegration, and bone regeneration.[8–10] However, there have been several reports on the detachment of hydroxyapatite from the Ti surface.[11] In addition, the biopolymer functionalization is time-consuming and laborious for further applications.[12]

Graphene is a 2D carbon material which has a sp^2 bonded honeycomb carbon structure. Graphene exhibits excellent electrical, physical, and optical properties,[13] making possible the applications to flexible and transparent electrical devices. Recently, graphene has been widely investigated for biomedical applications such as drug delivery systems,[14] biosensors,[15] and regenerative therapies. Especially, it is reported that graphene can improve the biocompatibility and promote the stem cell differentiation on the graphene surface for osteogensis,[16] neurogenesis,[17] and myogenesis.[18] Non-covalent interaction of RGO with proteins, growth factors, and differentiation inducers *via* π–π stacking, electrostatic, and hydrogen bonding can facilitate the stem cell differentiation, providing a facile preconcentration platform for cells.[16]

We previously reported facilitated differentiation of pre-osteoblasts on reduced graphene oxide (RGO) coated multi-pass caliber rolled Ti13Nb13Zr (MPCR-TNZ) alloy.[19] The drug loaded RGO coating on Ti surface provided progenitor cell stimulating microenvironment for rapid osseointegration. Osteogenic drug loaded RGO induced long-term cell stimulation by the high local concentration of osteogenic inducers on RGO surface. The drug loaded RGO enhanced the transcription of osteogenic markers such as Runt-related transcription factor 2, osteopontin, collagen type 1, and osteocalcin.[19] Here, we prepared commercially pure Ti (CP Ti) surface-modified with drug loaded RGO and characterized it by scanning electron microscopy (SEM), atomic force microscopy (AFM), energy dispersive spectrometry (EDS), X-ray photoelectron spectroscopy (XPS), high resolution TEM (HRTEM), and electron energy

[a]*Department of Materials Science and Engineering, Pohang University of Science and Technology (POSTECH), 77 Cheongam-ro, Nam-gu, Pohang, Kyungbuk 790-784, South Korea. E-mail: skhanb@postech.ac.kr*

[b]*Division of Integrative Biosciences and Biotechnology, Pohang University of Science and Technology (POSTECH), 77 Cheong-Am Ro, Nam-gu, Pohang, Kyungbuk 790-784, South Korea*

[c]*Graduate Institute of Ferrous Technology (GIFT), Pohang University of Science and Technology (POSTECH), 77 Cheongam-ro, Nam-gu, Pohang, Kyungbuk 790-784, South Korea*

[d]*Department of Mechanical Engineering, Korea Polytechnic University, 2121 Jeongwang-dong, Siheung-si, Gyeonggi-do 429-793, South Korea*

[e]*Department of Mechanical Engineering, Pohang University of Science and Technology (POSTECH), 77 Cheong-Am Ro, Nam-gu, Pohang, Kyungbuk 790-784, South Korea*

† Electronic supplementary information (ESI) available. See DOI: 10.1039/c6ra03905g

loss spectroscopy (EELS). After *in vitro* tests for cell viability, cellular attachment, and drug loading capability, *in vivo* bone regeneration on drug loaded RGO-CP Ti, RGO-CP Ti, and CP Ti were assessed in calvarial bone defect model rats. Detailed experimental methods are available in ESI.†

Fig. 1a shows a schematic illustration for the preparation of RGO-CP Ti. Mirror polished CP Ti was immersed in piranha solution for 1 h to introduce oxide layer on the surface of CP Ti. The oxidized CP Ti was immersed in 2% (3-aminopropyl)triethoxysilane (APTES) ethanol solution to prepare positively charged amine group on the surface. Then, negatively charged GO solution (pH 3) at a concentration of 4 mg mL^{-1} was poured on the APTES functionalized CP Ti for 5 min, and spin coated at 100 rpm for 2 s and at 2000 rpm for 30 s. Because APTES is positively charged below neutral pH and GO shows a negative charge at pH 3–9,[20] GO can be electrostatically bound to APTES–Ti. GO was evenly coated on APTES–Ti *via* electrostatic interaction. Finally, RGO-CP Ti was obtained by the chemical reduction of GO-coated CP Ti under hydrazine vapour exposure at 40 °C for 24 h. SEM images in Fig. 1b show the surface morphology of CP Ti and RGO-CP Ti. Bare CP Ti shows a flat and no significantly rough surface in both SEM and AFM images. After oxidization, the morphology in micro-scale showed pore-like structures and the surface roughness increased significantly due to the etching effect of piranha solution (Fig. S1†). After RGO coating, etched holes were covered with RGO layers, but the surface morphology remained similar with that of oxidized CP Ti (Fig. 1b). Nanoscale morphology of the RGO-CP Ti was also analyzed by AFM (Fig. 1c). Compared to CP Ti, RGO-CP Ti showed the typical graphene sheet like structures stacked as multi-RGO layers on the surface. The cross-sectional AFM image of RGO sheets stacked on CP Ti surface showed a height in the range of 1–4 nm (Fig. S2†).

The surface oxidization state of CP Ti, oxidized CP Ti, and APTES functionalized CP Ti was analyzed by EDS. As shown in Fig. 2a, CP Ti showed 3.66% oxygen content on the surface, which corresponded to titanium oxide layer on the outermost surface. After oxidization of CP Ti surface with a piranha solution, the oxygen content increased to 6.70% (Fig. 2b). The APTES functionalization increased the oxygen content to 13.02% and introduced 0.24% of Si on the surface (Fig. 2c). However, nitrogen peak (Kα = 0.392) was not distinguished from Ti peak (Lα = 0.452) due to its low content compared to Ti and similar characteristic X-ray peak position. After electrostatic adhesion of GO on APTES functionalized CP Ti, carbon chemical state was analyzed by XPS. GO coated CP Ti showed typical

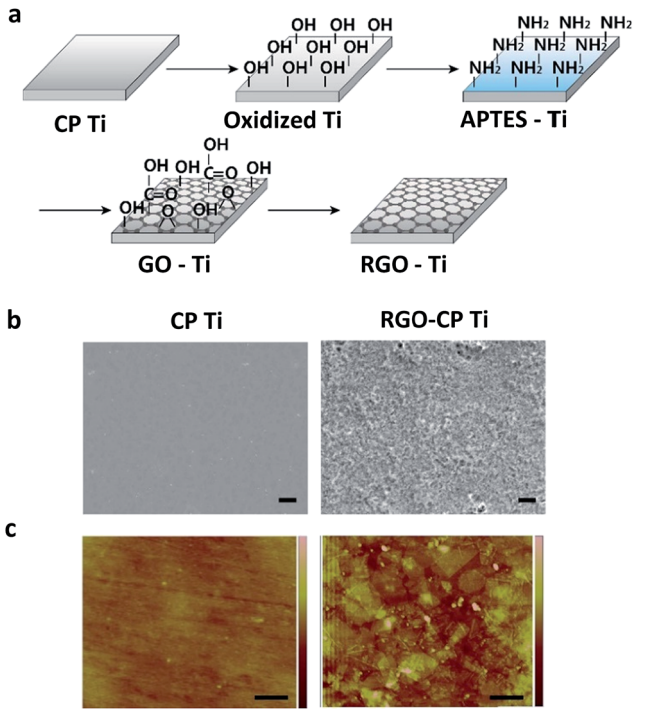

Fig. 1 (a) Schematic illustration for the preparation of RGO-CP Ti. (b) SEM images of CP Ti and RGO-CP Ti (scale bar = 2 μm). (c) AFM images of CP Ti and RGO-CP Ti (scale bar = 500 nm).

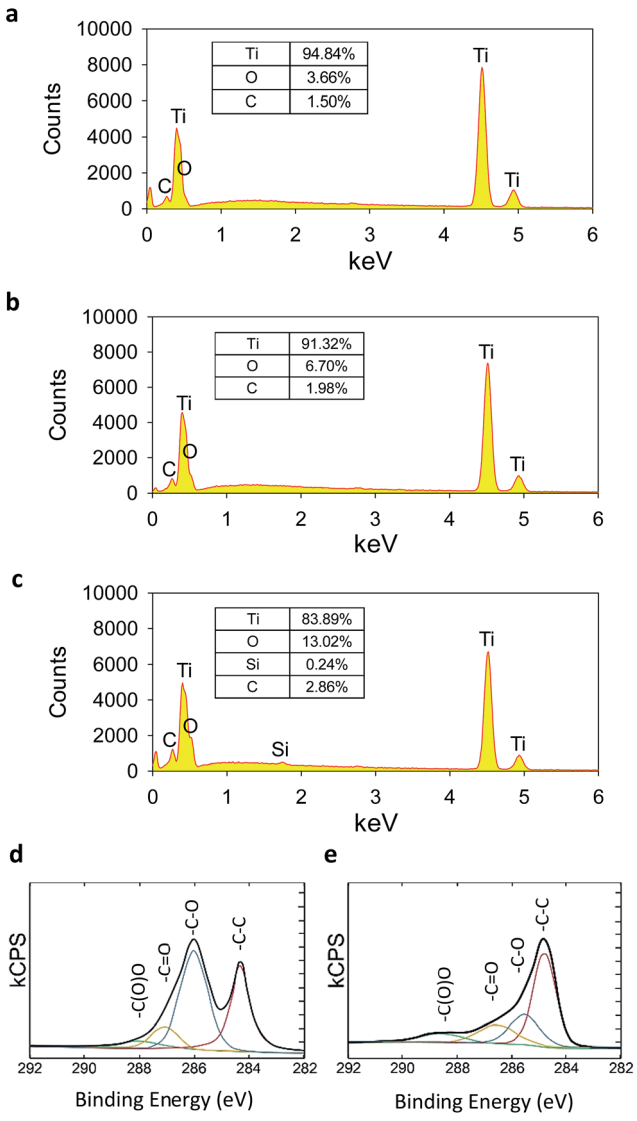

Fig. 2 EDS elementary analysis of (a) CP Ti, (b) oxidized CP Ti, and (c) APTES functionalized CP Ti. XPS analysis of carbon chemical state of (d) GO-CP Ti and (e) RGO-CP Ti.

GO peak composed of various oxidized carbon states on the graphitic domain including C–O, C═O, and C(O)O peaks (Fig. 2d). After chemical reduction of GO coated CP Ti (GO-CP Ti), XPS spectrum showed the reduced oxidized carbon states confirming the successful RGO coating on CP Ti surface (Fig. 2e). Contact angle measurement of RGO-CP Ti and CP Ti was conducted for the analysis of surface hydrophilicity. CP Ti surface showed contact angle of 44.2°, whereas RGO-CP Ti showed 78.4°. RGO coating resulted in hydrophobic surface due to the reduction of surface oxides (Fig. S3†).[19]

HRTEM and EELS mapping of RGO-CP Ti were performed after sample preparation using a focused ion beam (FIB) by the conventional lift-off technique. The interface was composed of three layers including carbon-rich layer, Ti-oxide middle layer, and Ti matrix inner layer (Fig. 3a). Although Ti oxide layer was formed roughly, the interface between the carbon-rich outer layer and Ti-oxide layer were flat. EELS mapping clearly showed Ti (blue), oxygen (green) and carbon (red) layers on the image (Fig. 3b). Ti mapping shows a strong Ti signal at the bottom, but a relatively weak signal in the middle part corresponding to Ti oxide (Fig. 3c). Oxygen mapping shows a high oxygen content in Ti oxide region, but a low content of oxygen in RGO layer corresponding to the remaining oxide in RGO. The carbon-rich outer layer was formed by RGO coating with a uniform thickness of 10 nm, which might result from the stacking of graphene multi-layers during the coating process. From the results, we could estimate that about 10 layers of RGO were stacked on CP Ti, considering *ca.* 1 nm thickness of the single RGO layer. The low carbon signal from Pt–C protecting layer could be distinguished from that of graphene multi-layers.

The drug loading capability of RGO-CP Ti was assessed using osteogenic chemical drugs such as dexamethasone (DEX) and ascorbic acid (AA). Also, protein adsorption was assessed using bovine serum albumin (BSA). DEX or AA at a concentration of 100 μg mL^{-1} was loaded on RGO-CP Ti surface for 1 h and the supernatant was harvested for drug loading content analysis. As shown in Fig. 4a, 5.74% of Dex and 3.10% of AA was loaded on the RGO-CP Ti surface. Because DEX and AA have π electrons on the structure, they can be loaded on the graphitic domain of RGO surface through π–π stacking.[20] BSA at a concentration of 1 mg mL^{-1} was loaded on the RGO-CP Ti for 1 h and the protein concentration in the supernatant was analyzed by UV-vis spectroscopy. After 1 h, 25% of the protein could be loaded on the RGO-CP Ti. Each test was conducted with 4 samples measuring at least 5 times.

The viability of pre-osteoblast MC3T3-E1 cells on CP Ti and RGO-CP Ti was assessed by MTT assay after culture for 3 days. Cells on RGO-CP Ti showed higher cell viability than those on CP Ti (Fig. 4b). It is generally considered that hydrophilic surface provides biocompatible environment compared to hydrophobic surface. However, in the case of RGO, it was reported that rapid absorption of serum protein on RGO made biocompatible and hydrophilic environment for cell adhesion and proliferation.[19] As shown in fluorescence image of F-actin stained cells, cells on RGO-CP Ti showed well spreaded and attached morphology compared with those on CP Ti after 3 days (Fig. 4c and d). Cell adhesion area was determined by measuring the region of F-actin fluorescence and averaged per one cell using image J software after adjustment of image scale (Fig. 4e).

On the basis of our previous investigation on facilitated preosteoblast differentiation on drug loaded RGO-CP Ti *in vitro*, we carried out *in vivo* osseointegration test after implantation of RGO-CP Ti onto the calvarial bone defect of Sprague Dawley (SD) rats. Bone tissue regenerated on the surface was visualized by synchrotron X-ray imaging. CP Ti as a control, RGO-CP Ti, and Dex/RGO-CP Ti were inserted in the calvarial bone defect of SD rats and then sutured for the bone regeneration assessment. After 8 weeks, the calvarial tissues were harvested and fixed in 10% formaldehyde solution at 4 °C for a day. As shown in Fig. 5, bone regeneration initiated from the edge of the inserted titanium surface. The critical bone defect size of rat calvaria is

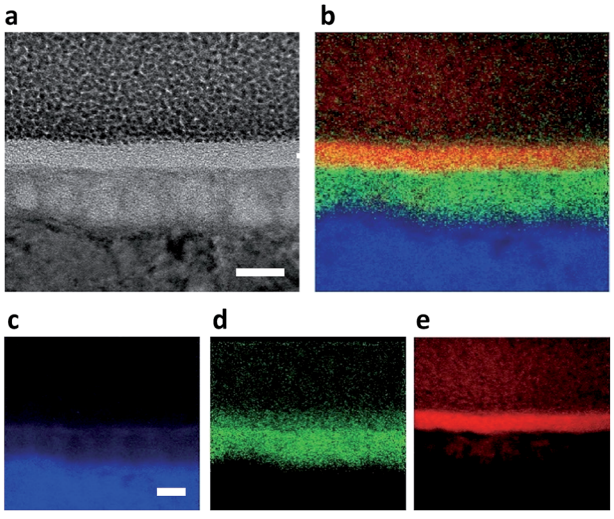

Fig. 3 (a) HRTEM image of RGO-CP Ti. (b) EELS mapping of RGO-CP Ti, where (c) titanium in blue, (d) oxygen in green, and (e) carbon in red (arrows indicate carbon rich RGO, scale bar = 20 nm).

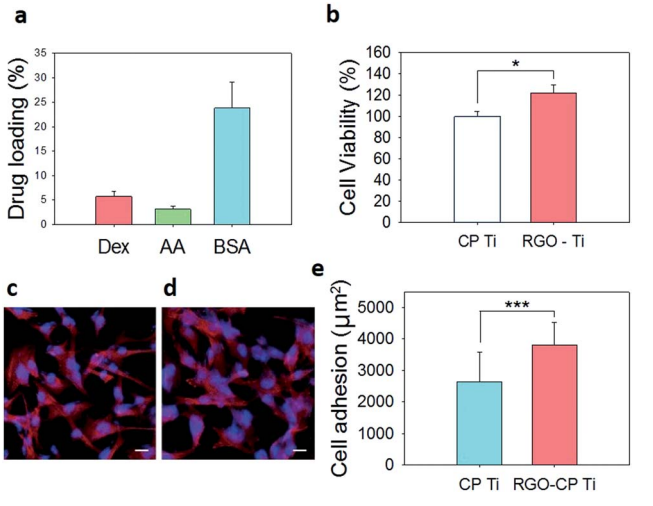

Fig. 4 (a) Drug loading (%) on RGO-CP Ti. (b) Relative cell viability on CP Ti and RGO-CP Ti. Confocal microscopic images of F-actin stained preosteoblasts on (c) CP Ti and (d) RGO-CP Ti (scale bar = 25 μm). (e) Cell adhesion area determined from the region of F-actin fluorescence (*$P \leq 0.05$ and ***$P \leq 0.001$).

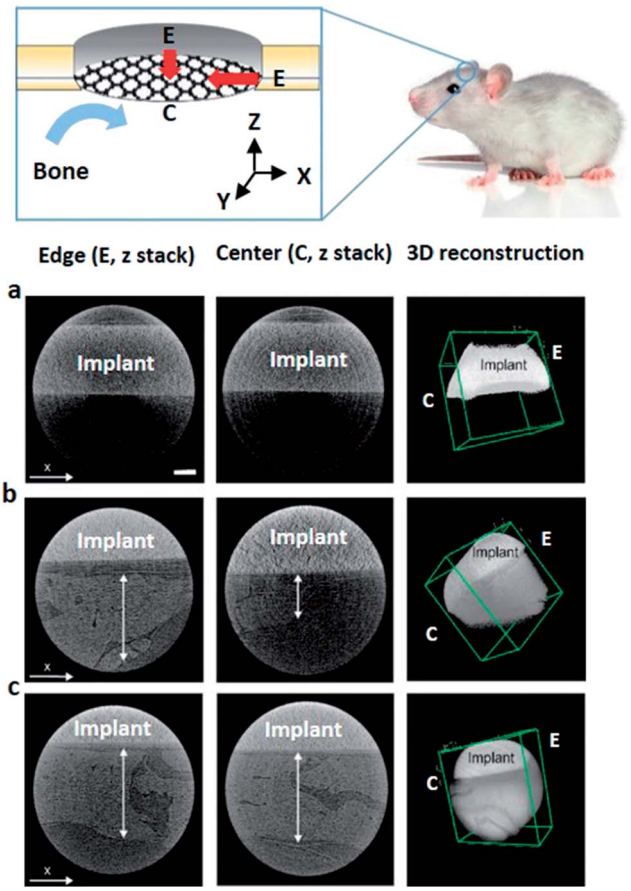

Fig. 5 Synchrotron X-ray images of regenerated bones on (a) CP Ti, (b) RGO-CP Ti, and (c) Dex/RGO-CP Ti after 8 weeks (scale bar = 200 μm). Vertical arrow indicates bone thickness (*z*-axis fixed, z-stacked image of edge part (left column) and central part (center column) of regenerated bone on the implant).

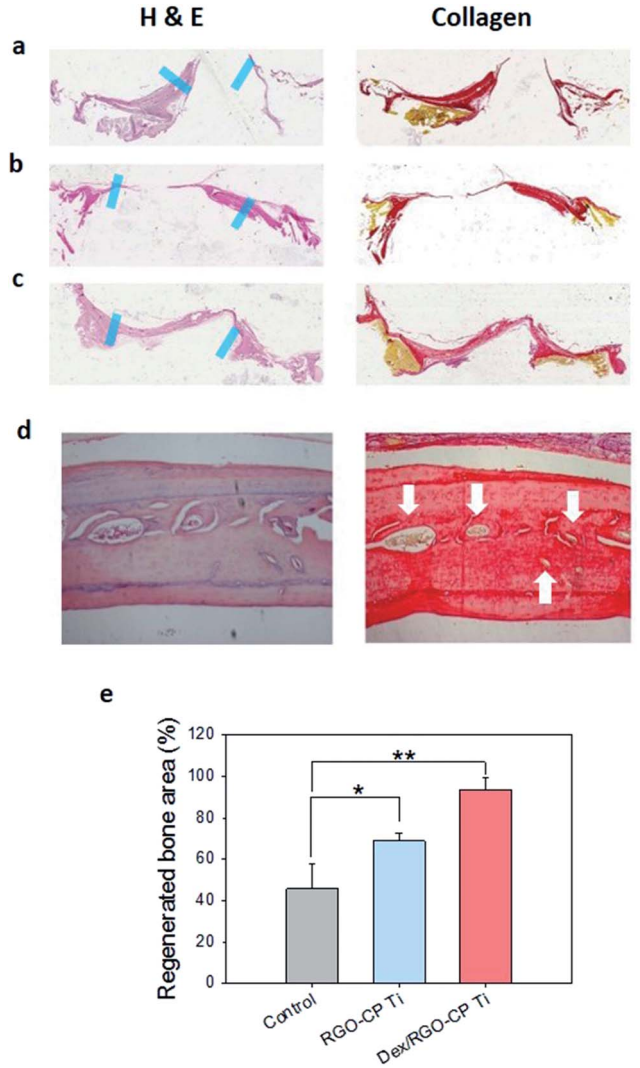

Fig. 6 Histological analysis of regenerated bones after H&E and collagen staining on (a) CP Ti, (b) RGO-CP Ti, and (c) Dex/RGO-CP Ti. Blue mark indicates initial edge of bone defect. (d) Magnified image of bone tissue regenerated on Dex/RGO-CP Ti. Arrows indicate collagen type I (magnification = 10×). (e) Relative regenerated bone area (*$P \leq 0.05$ and **$P \leq 0.01$).

generally regarded as 8 mm in the bone regeneration study.[21] The left column indicates left edges and the middle column indicates the central parts of regenerated bones on the implants. CP Ti resulted in no significant bone regeneration from the edge to the center of the surface. In the case of RGO-CP Ti, thick bone was observed at the edge, but incomplete bone regeneration at the center of the surface. However, in the case of Dex/RGO-CP Ti, significant bone regeneration and compact osseointegration of regenerated bone was observed in the entire region from the edge to the center of the implant surface.

Histological analysis was performed for bones regenerated on CP Ti, RGO-CP Ti, and Dex/RGO-CP Ti using hematoxylin and eosin (H&E), and collagen staining kits. CP-Ti showed no significant bone regeneration between the edge of the carvarial bone defect (Fig. 6a). RGO-CP Ti showed non-matured and relatively thin regenerated bone tissue on the surface (Fig. 6b). In the case of Dex/RGO-CP Ti, however, uniform bone regeneration was clearly observed from the edge to the center of the calvaria. Also, osteocytes in the bone matrix was observed on the regenerated bone tissues (Fig. 6c and d). Collagen staining showed that a significant amount of collagen type I (yellow) was formed in bone tissues regenerated on Dex/RGO-CP Ti. It is the main component of bone matrix.

Regenerated bone area was calculated using image J program after adjustment of the scale. Photoimages clearly showed more efficient and matured bone tissue regeneration on Dex/RGO-CP Ti than those on RGO-CP Ti and CP Ti (Fig. S4†). The regenerated bone area was calculated based on 8 mm diameter of the initial bone defect. Regenerated bone area was 45.65% for CP Ti, 68.72% for RGO-CP Ti, and 93.38% for Dex/RGO-CP Ti (Fig. 6e). All these data successfully confirmed that RGO-CP Ti worked as an effective drug carrier and drug loaded RGO-CP Ti greatly promoted the bone regeneration and osseointegration after *in vivo* implantation to SD rats.

The rapid osseointegration on the implant surface can be greatly beneficial to patients by reducing the period of therapy.

Obviously, graphene materials have several advantages for the bone regeneration therapy. Graphene can be used for facile high amount drug loading *via* π–π stacking and hydrophobic interaction.[16] Also, we previously reported stable drug loading and long-term Dex release from the RGO surface for a week.[19] Because bone regeneration therapy requires several weeks for osseointegration, long term drug release from the implant surface would be greatly beneficial for cell stimulation to enhance bone regeneration.[19] Furthermore, it was reported that graphene based materials such as GO and RGO show antibacterial activity, posing membrane stress and oxidative stress onto bacterial cells.[22,23] Taken together, we could confirm the feasibility of graphene coated Ti implant materials for the applications to effective bone regeneration.

Conclusions

The surface-modification of CP Ti was successfully performed using drug loaded RGO for accelerated bone tissue regeneration. HRTEM and EELS mapping clearly visualized the interface of three layers including carbon-rich outer layer, Ti-oxide middle layer, and Ti matrix inner layer. Due to drug loading capability of graphene surface, osteogenic inducers could be loaded on the graphitic domain of the RGO-CP Ti. After *in vitro* tests, we could confirm the effective bone regeneration and the osseointegration on Dex loaded RGO-CP Ti in the calvarial bone defect of SD rats by synchrotron X-ray imaging and histological analysis with H&E and collagen staining. The facile surface modification of Ti implant with drug loaded graphene can be exploited for various bone tissue engineering applications.

Acknowledgements

This work was financially supported by POSCO. This work was also financially supported by Bio & Medical Technology Development Program (Project No. 2012M3A9C6049791) of the National Research Foundation by the Korean government (MEST). This research was supported by a grant of the Korean Health Technology R&D Project, Ministry of Health and Welfare, Korea (HI14C1658).

Notes and references

1 N. T. C. Oliveira and A. C. Guastaldi, Electrochemical stability and corrosion resistance of Ti–Mo alloys for biomedical applications, *Acta Biomater.*, 2009, **5**, 399–405.

2 H. E. Achneck, R. M. Jamiolkowski, A. E. Jantzen, J. M. Haseltine, W. O. Lane, J. K. Huang, L. J. Galinat, M. J. Serpe, F. H. Lin, M. Li, A. Parikh, L. Ma, T. Chen, B. Sileshi, C. A. Milano, C. S. Wallace, T. V. Stabler, J. D. Allen, G. A. Truskey and J. H. Lawson, The biocompatibility of titanium cardiovascular devices seeded with autologous blood-derived endothelial progenitor cells: EPC-seeded antithrombotic Ti implants, *Biomaterials*, 2011, **32**, 10–18.

3 T. A. Petriea, J. E. Raynor, C. D. Reyes, K. L. Burns, D. M. Collard and A. J. García, The effect of integrin-specific bioactive coatings on tissue healing and implant osseointegration, *Biomaterials*, 2008, **29**, 2849–2857.

4 Y. T. Sul, B. S. Kang, B. Johansson, H. S. Um, C. J. Park and T. Albrektsson, The roles of surface chemistry and topography in the strength and rate of osseointegration of titanium implants in bone, *J. Biomed. Mater. Res., Part A*, 2009, **89**, 942–950.

5 C. N. Elias, Y. Oshida, J. H. C. Lima and C. A. Muller, Relationship between surface properties (roughness, wettability and morphology) of titanium and dental implant removal torque, *J. Mech. Behav. Biomed. Mater.*, 2008, **1**, 234–242.

6 Y. Gao, S. Zou, X. Liu, C. Bao and J. Hu, The effect of surface immobilized bisphosphonates on the fixation of hydroxyapatite-coated titanium implants in ovariectomized rats, *Biomaterials*, 2009, **30**, 1790–1796.

7 S. E. Kim, S. H. Song, Y. P. Yun, B. J. Choi, I. K. Kwon, M. S. Bae, H. J. Moon and Y. D. Kwon, The effect of immobilization of heparin and bone morphogenic protein-2 (BMP-2) to titanium surfaces on inflammation and osteoblast function, *Biomaterials*, 2011, **32**, 366–373.

8 D. S. Hwang, J. H. Waite and M. Tirrell, Promotion of osteoblast proliferation on complex coacervation-based hyaluronic acid – recombinant mussel adhesive protein coatings on titanium, *Biomaterials*, 2010, **31**, 1080–1084.

9 D. W. Lee, Y. P. Yun, K. Park and S. E. Kim, Gentamicin and bone morphogenic protein-2 (BMP-2)-delivering heparinized-titanium implant with enhanced antibacterial activity and osteointegration, *Bone*, 2012, **50**, 974–982.

10 E. Anitua, G. Orive, R. Pla, P. Roman, V. Serrano and I. Andia, The effects of PRGF on bone regeneration and on titanium implant osseointegration in goats: a histologic and histomorphometric study, *J. Biomed. Mater. Res., Part A*, 2009, **91**, 158–165.

11 G. Schmidmaier, B. Wildemann, P. Schwabe, R. Stange, J. Hoffmann, N. P. Sudkamp, N. P. Haas and M. Raschke, A new electrochemically graded hydroxyapatite coating for osteosynthetic implants promotes implant osteointegration in a rat model, *J. Biomed. Mater. Res., Part A*, 2002, **63**, 168–172.

12 W. B. Tasi, C. Y. Chien, H. Thissen and J. Y. Lai, Dopamine-assisted immobilization of poly(ethylene imine) based polymers for control of cell–surface interactions, *Acta Biomater.*, 2011, **7**, 2518–2525.

13 H. S. Jung, W. H. Kong, D. K. Sung, M. Y. Lee, S. E. Beack, D. H. Keum, K. S. Kim, S. H. Yun and S. K. Hahn, Nanographene oxide–hyaluronic acid conjugate for photothermal ablation therapy of skin cancer, *ACS Nano*, 2014, **8**, 260–268.

14 X. Sun, Z. Liu, K. Welsher, J. T. Robinson, A. Goodwin, S. Zaric and H. Dai, Nano-Graphene Oxide for Cellular Imaging and Drug Delivery, *Nano Res.*, 2008, **1**, 203–212.

15 M. S. Mannoor, H. Tao, J. D. Clayton, A. Sengupta, D. L. Kaplan, R. R. Naik, N. Verma, F. G. Omenetto and M. C. McAlpin, Graphene-based wireless bacteria detection on tooth enamel, *Nat. Commun.*, 2012, **3**, 763.

16 W. C. Lee, C. H. Y. X. Lim, H. Shi, L. A. L. Tang, Y. Wang, C. T. Lim and K. P. Loh, Origin of enhanced stem cell growth and differentiation on graphene and graphene oxide, *ACS Nano*, 2011, **5**, 7334–7341.

17 S. Y. Park, J. Park, S. H. Sim, M. G. Sung, K. S. Kim, B. H. Hong and S. Hong, Enhanced Differentiation of Human Neural Stem Cells into Neurons on Graphene, *Adv. Mater.*, 2011, **23**, H263–H267.

18 S. H. Ku and C. B. Park, Myoblast differentiation on graphene oxide, *Biomaterials*, 2013, **34**, 2017–2023.

19 H. S. Jung, T. Lee, I. K. Kwon, H. S. Kim, S. K. Hahn and C. S. Lee, Surface Modification of Multipass Caliber-Rolled Ti Alloy with Dexamethasone-Loaded Graphene for Dental Applications, *ACS Appl. Mater. Interfaces*, 2015, **7**, 9598–9607.

20 H. S. Jung, M. Y. Lee, W. H. Kong, I. H. Do and S. K. Hahn, Nano graphene oxide–hyaluronic acid conjugate for target specific cancer drug delivery, *RSC Adv.*, 2014, **4**, 14197–14200.

21 P. P. Spicer, J. D. Kretlow, S. Young, J. A. Jansen, F. K. Kasper and A. G. Mikos, Evaluation of bone regeneration using the rat critical size calvarial defect, *Nat. Protoc.*, 2012, **7**, 1918–1929.

22 S. Liu, T. H. Zeng, M. Hofmann, E. Burcombe, J. Wei, R. Jiang, J. Kong and Y. Chen, Antibacterial Activity of Graphite, Graphite Oxide, Graphene Oxide, and Reduced Graphene Oxide: Membrane and Oxidative Stress, *ACS Nano*, 2011, **5**, 6971.

23 W. B. Hu, C. Peng, W. J. Luo, M. Lv, X. M. Li, D. Li, Q. Huang and C. H. Fan, Graphene-Based Antibacterial Paper, *ACS Nano*, 2010, **4**, 4317–4323.

